Structure of Cu_B in the Binuclear Heme−Copper Center of the Cytochrome aa_3-Type Quinol Oxidase from *Bacillus subtilis*: An ENDOR and EXAFS Study†

Yang C. Fann,‡ Ishak Ahmed,§ Ninian J. Blackburn,|| John S. Boswell,|| Marina L. Verkhovskaya,§ Brian M. Hoffman,‡ and Mårten Wikström*,§

Department of Chemistry, Northwestern University, Evanston, Illinois 60208-3113, Helsinki Bioenergetics Group, Institute of Biomedical Sciences, Department of Medical Chemistry, 00014 University of Helsinki, Helsinki, Finland, and Department of Chemistry, Biochemistry and Molecular Biology, Oregon Graduate Institute of Science and Technology, Portland, Oregon 97291

Received April 25, 1995; Revised Manuscript Received June 14, 1995⊗

ABSTRACT: We have studied the structure of the Cu_B site in the binuclear heme−copper center of the fully oxidized form of the quinol-oxidizing cytochrome aa_3-600 from *Bacillus subtilis* by EXAFS and ENDOR spectroscopy. This enzyme is member of the large superfamily of heme−copper respiratory oxidases, which catalyze the reduction of dioxygen to water and link it to translocation of protons across the bacterial or mitochondrial membrane. The EXAFS of the Cu_B site strongly suggests tetragonal coordination by two or three histidines with one or two O/N donor ligands. There are some indications that a Cl^- ion might fractionally occupy substitution-labile sites, although the majority of enzyme molecules did not contain any heavy (second row) scatterers, indicative of a Cl^- (or S) bridge between the heme iron and Cu_B [cf. Powers, L., *et al.* (1994) *Biochim. Biophys. Acta 1183*, 504−512]. Proton ENDOR spectroscopy of the Cu_B site in ^1H_2O and ^2H_2O media showed evidence of an oxygenous copper ligand with an exchangeable proton. ^{14}N ENDOR revealed three inequivalent nitrogenous ligands with hyperfine coupling constants consistent with histidines. Together, these results strongly suggest that the fully oxidized enzyme has a low-symmetry, tetragonal Cu_B site with three histidine nitrogens and one oxygen as ligands, the latter with an exchangeable proton(s). The identity and assignment of these ligands are discussed.

The respiratory heme−copper oxidases constitute a superfamily of proton-translocating terminal oxidases in both prokaryotic organisms and the mitochondria of eukaryotic cells (see Saraste, 1990; Hosler et al., 1993; Calhoun et al., 1994). The most widely studied enzyme is the cytochrome *c* oxidase of mammalian mitochondria, but its 13-subunit composition and nonamenability to mutagenesis have hampered progress in its structural characterization. On the other hand, a number of bacterial heme−copper oxidases contain only three subunits, which are homologous to the mtDNA-encoded large subunits in the mitochondrial enzyme and exhibit catalytic characteristics similar to the latter.

The cytochrome *c* oxidases contain three redox centers, Cu_A,[1] heme Fe_a, and the binuclear, dioxygen-binding heme Fe_{a3}−Cu_B center, and utilize cytochrome *c* as the electron donor. A second major branch of this enzyme family uses ubiquinol or menaquinol as the reducing substrate, and in these cases the Cu_A center is absent. Such enzymes are the cytochrome bo_3 of *Escherichia coli* (Puustinen et al., 1991, 1992; Minghetti et al., 1992; Hosler et al., 1993; Calhoun et al., 1994) and cytochrome aa_3-600 of *Bacillus subtilis* (Lauraeus et al., 1991, 1992; Santana et al., 1992), which is the subject of the present study. Many bacteria can be induced to produce a certain terminal oxidase when grown under specified conditions. Thus, *B. subtilis* can be induced to produce a cytochrome caa_3-type cytochrome *c* oxidase in addition to cytochrome aa_3-600, when grown aerobically on a nonfermentable carbon source, whereas cytochrome aa_3-600, apparently the constitutive respiratory oxidase, is virtually the only one expressed during logarithmic growth on a fermentable substrate (Lauraeus et al., 1991).

There is remarkable sequence homology between subunits I of all members of the superfamily, and it is established that the binuclear heme Fe_{a3}−Cu_B dioxygen reduction site resides within this subunit, together with the low-spin heme Fe_a, while the Cu_A center is located in subunit II. Spectroscopic and site-directed mutagenesis, as well as three-dimensional modeling, has led to a working model (Hosler et al., 1993) for the basic structure of the Fe_{a3}−Cu_B center and its connectivity to Fe_a. Figure 1 shows one version of this model in which the distance between the heme edges is about 11 Å to account for the measured rate of heme−heme electron transfer (Verkhovsky et al., 1992).

According to this model, the metal centers of subunit I are coordinated by fully conserved histidine residues: Fe_a is coordinated to His102 from transmembrane helix II and to His421 on one side of helix X. His419 on the opposite side of helix X is the proximal ligand of Fe_{a3}, the distal side facing the Cu_B site. Cu_B is coordinated to His333 and His334

† This work was supported by grants from the Sigrid Jusèlius Foundation, the Academy of Finland (M.R.C.), the University of Helsinki (to M.W.), and the National Institutes of Health (HL 13531 to B.M.H. and NS 27583 to N.J.B.).

* Address correspondence to this author at Department of Medical Chemistry, P.O. Box 8, 00014 University of Helsinki, Helsinki, Finland.

‡ Northwestern University.

§ University of Helsinki.

|| Oregon Graduate Institute of Science and Technology.

⊗ Abstract published in *Advance ACS Abstracts,* August 1, 1995.

[1] Abbreviations: Fe_a, low−spin heme iron (cytochrome *a*); Fe_{a3}, oxygen-reactive heme iron of the binuclear center (cytochrome a_3); Cu_B, copper of the binuclear center; Cu_A, electron input copper center of cytochrome *c* oxidases; EXAFS, extended X-ray absorption fine structure; ENDOR, electron−nuclear double resonance.

0006-2960/95/0434-10245$09.00/0

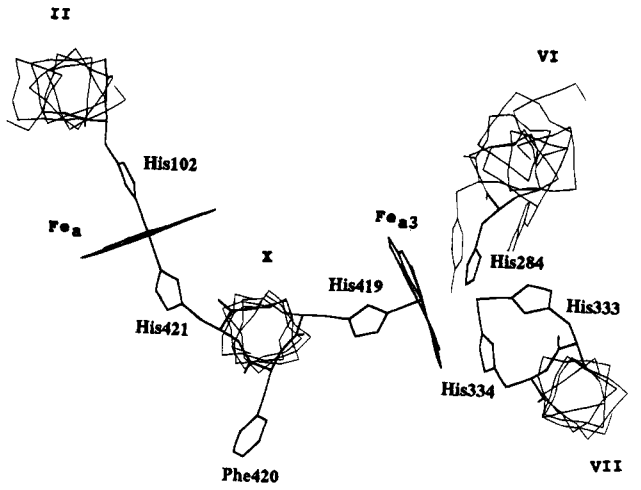

FIGURE 1: Model of the arrangement of the Fe_a, Fe_{a3}, and Cu_B centers in the heme–copper respiratory oxidase superfamily.[2] Transmembranous helices II, VI, VII, and X, with their associated metal centers, are viewed from the periplasmic side (outside) of the membrane, perpendicular to the membrane plane. The metal ligand histidines are highlighted. In addition, the well-conserved residues Phe420 in helix X and Trp280 and Tyr288 in helix VI are shown. The through-bond pathway connecting Fe_a with Fe_{a3} is highlighted, and the shortest distance between the heme edges is about 11 Å.

of the putative transmembrane helix VII, and possibly to His284 in helix VI as well. Recent mutagenesis studies have also suggested that Tyr288 (in helix VI) might be a ligand to Cu_B in certain states of the enzyme, since its mutation to Phe destroys the CO-binding capacity at the reduced Cu_B site (Thomas et al., 1994).

The binuclear Fe_{a3}–Cu_B center is the site of dioxygen chemistry in all of these enzymes. Moreover, it seems clear that this site is also intimately involved in the proton-translocating function (Wikström, 1989), and several different models of proton-translocating mechanisms have been proposed, all of which have the Fe_{a3}–Cu_B center structure in common (Chance & Powers, 1985; Mitchell, 1987, 1988; Wikström, 1988; Rousseau et al., 1993; Woodruff, 1993; Babcock & Wikström, 1992; Wikström et al., 1994; Morgan et al., 1994; Rich, 1995). From this it is clear that the structural information of the binuclear site is of great importance in order to gain an understanding of the proton translocation mechanism, as well as of the catalytic mechanism of dioxygen reduction.

The two metals of the binuclear Fe_{a3}–Cu_B center are within 5 Å from one another in the oxidized enzyme and form a normally EPR-undetectable spin-coupled pair (van Gelder & Beinert, 1969). The coupling is thought to be mediated by a bridging ligand, the nature of which is still under debate. EPR signals are observed from the binuclear center when either of the two metals is reduced or when the magnetic coupling has been broken by other means. In redox equilibrium titrations, Cu_B is always reduced before Fe_{a3}, yielding high-spin ferric signals from the latter, with Cu_B remaining EPR-invisible (see Wikström et al., 1981). However, intermediate states have been trapped during turnover of the enzyme that show rhombic EPR signals from cupric Cu_B (Reinhammar et al., 1980; Karlsson et al., 1981). An ENDOR study of such a trapped state suggested that Cu_B may have three nitrogenous (histidine) ligands and a fourth unknown ligand (Cline et al., 1983). The latter may be the putative bridging ligand in the oxidized state of the center or another (solvent) molecule replacing it. EPR studies have also demonstrated that a water or hydroxide molecule derived from O_2 is coordinated to Cu_B in a trapped intermediate state of the catalytic cycle (Hansson et al., 1982).

Most EXAFS studies on the oxidized binuclear site reported to date have been done on the mitochondrial enzyme and have suggested two or three (Powers et al., 1981; Li et al., 1987) nitrogenous ligands of Cu_B, plus one S/Cl ligand presumed to bridge Cu_B with Fe_{a3}. A preliminary Fe EXAFS report by Scott et al. (1988) indicated that the putative bridging ligand was lost in chloride-free conditions, but to our knowledge there has been no followup on this issue. Earlier EXAFS work was hampered by the fact that the mitochondrial cytochrome *c* oxidase also contains a Cu_A site, which, by itself, is now known to contain two copper ions (Lappalainen et al., 1993). For this reason, EXAFS studies of the structurally homologous quinol oxidases appear more promising, since these enzymes lack the Cu_A center and its ligands altogether. Recently, Powers et al. (1994) studied the quinol-oxidizing cytochrome aa_3-600 from *B. subtilis* and reported EXAFS data very similar to those reported previously with the mitochondrial enzyme. A heavy S/Cl scatterer was observed bridging the metals, the identity of which was considered to be chloride since no conserved cysteines or methionines could conceivably provide a sulfur and since no acid-labile sulfur was detected.

Here, we have continued the study of the structure of the Cu_B site of the *B. subtilis* cytochrome aa_3-600 by both EXAFS and ENDOR techniques, with the aim of resolving the long-standing problem of the identity of the bridging ligand and the putative role of Cl^- as such a ligand, as well as exploring the coordination sphere of Cu_B more generally.

MATERIALS AND METHODS

Enzyme Samples and Chloride Determination. Cytochrome aa_3-600 from *B. subtilis* was isolated and purified as described previously (Lauraeus et al., 1991). The enzyme concentration was determined from the dithionite-reduced minus air-oxidized optical difference spectrum at the wavelength couple 600–626 nm, using a millimolar absorptivity of 26.4 cm^{-1} for the two-heme enzyme unit (Lauraeus et al., 1992).

Samples for ENDOR spectroscopy were prepared as follows: a 0.1 mM suspension of cytochrome aa_3-600 (in 50 mM Tris, 150 mM NaCl, and 0.5% Triton X-100, pH 8) was diluted 4 times in buffer containing 100 mM glycine and 150 mM NaCl (pH 8.8). This was then concentrated to the original volume using Amicon Centricon-100 microconcentrators. This process of dilution and subsequent concentration was repeated three times to ensure that the final sample was at pH 8.8. For samples in heavy water, the enzyme dilution was done in the same glycine buffer as before, except that the buffer was made up in ^2H_2O at pD 8.8 (pH-meter reading 8.4), and concentrated as before. The procedure was repeated three times to ensure that the ^2H_2O content exceeded 90%.

[2] Note Added in Proof: The recently solved crystal structure of the aa_3-type cytochrome *c* oxidase from *P. denitrificans* (S. Iwata, Ch. Ostermeier, B. Ludwig, and H. Michel, Nature, submitted for publication) suggests that the positions of helices VI and VII should be interchanged in Figures 1 and 11.

Samples for EXAFS spectroscopy were prepared as follows: 2% (w/v) potassium cholate was added to about 35 μM enzyme in 50 mM Tris, 150 mM NaCl, and 0.3% Triton X-100 (pH 8.0). This suspension was 50% saturated with ammonium sulfate by adding saturated, neutralized ammonium sulfate solution to precipitate the enzyme. The precipitate was dissolved in buffer containing 50 mM Tris, 150 mM NaCl, 0.1% Triton X-100, and 10% glycerol (pH 8.0; the concentration of cytochrome aa_3-600 was about 0.35 mM in this stock solution).

To prepare the *high-pH sample* (pH 8.8), about 0.15 mL of stock enzyme solution was diluted 4 times in buffer containing 100 mM glycine, 150 mM NaCl, and 20% (v/v) glycerol (pH 8.8). This was then concentrated as before, and the process of dilution and concentration was repeated three times to ensure that the pH was 8.8 in the final preparation.

The *chloride-free samples* were prepared as follows: 0.2 mM stock enzyme solution was dialyzed overnight against 0.5 L of Cl-free buffer (50 mM Tris, 75 mM Na_2SO_4, 0.1% Triton X-100, and 20% (v/v) glycerol, pH 8.0). The external buffer was changed and dialysis continued for 5 h against 0.5 L of new buffer. The volume of the sample increased upon dialysis and was concentrated as before to a final concentration between 0.2 and 0.3 mM. The concentration of Cl^- in the enzyme suspension was determined using a Spectroquant kit (Merck Cl^- 14755) and was found to be <5 μM. This Cl^- assay is based on the reaction of chloride with mercuric thiocyanate in the presence of ferric ions to form mercuric chloride, chloromercurate(II) anion, and orange-red ferric thiocyanate. Since salts and sugars influence the color, a calibration curve had to be made with fresh dialysis medium.

In an attempt to determine Cl^- that might be tightly bound to the enzyme, the dialysis bag was boiled in alkaline conditions for 10 min after completion of dialysis, the suspension was acidified, and the protein was sedimented and filtered on a Centricon column. Then Cl^- was determined from the solution as before, and the concentration was found to be <5 μM in enzyme suspensions of 0.2−0.3 mM.

ENDOR Measurements. ENDOR spectra were recorded with a Varian E109 continuous-wave (CW) EPR spectrometer equipped with an E110 35 GHz microwave bridge using 100 kHz field modulation, as described previously (Werst et al., 1991). To enhance the ENDOR response, the radiofrequency (RF) output of the PTS 160 RF synthesizer was band-broadened by mixing with a white noise generator, the bandwidth of which was about 100 kHz (Hoffman et al., 1994). This is particularly useful for low-concentration protein samples.

For protons (^{1}H, $I = {}^1/_2$), the ENDOR spectrum of a frozen solution corresponds to one or more doublets ($\nu_\pm$) centered at its Larmor frequency [$\nu(^1\text{H})$] and split by the hyperfine coupling $A(^1\text{H})$: $\nu = |\nu(^1\text{H}) \pm A(^1\text{H})/2|$ (Hoffman et al., 1993). The frozen solution ENDOR spectrum for a nucleus (n) of spin $I = 1$, such as ^{14}N or ^{2}H, is, in principle, a quartet given by the equation

$$\nu_{\pm(\pm)} = |\pm A(n)/2 + \nu(n) \pm 3P(n)/2| \qquad (1)$$

where $A(n)$ and $P(n)$ are the orientation-dependent hyperfine and quadrupole coupling constants, respectively, and $\nu(n)$ is the field-dependent nuclear Larmor frequency. For ^{14}N nuclei of Cu_B at Q band, $A(^{14}\text{N})/2 > \nu(^{14}\text{N}) \sim 3.5$ MHz $> 3P(^{14}\text{N})/2$, and eq 1 describes a doublet centered at $A(^{14}\text{N})/2$ and split by $2\nu(^{14}\text{N})$, with further splitting by the quadrupole term, if resolved. For Cu-bound histidine, the quadrupole interaction commonly is not resolved, and it is important to note that the maximum possible quadrupole splitting of a metal-coordinated histidyl nitrogen is $3P_{max} \sim 3.3$−3.5 MHz (Gurbiel et al., 1993). When the quadrupole splittings are not resolved from $I = 1$, we suppress the second $\pm$ symbol.

Table 1: Experimental Parameters Used in Data Collection

	normal	chloride-free	high pH
synchrotron source	NSLS	NSLS	SSRL
beam energy (GeV)	2.5	2.5	3.0
stored current range (mA)	220−100	220−100	110−40
beamline	X9	X9	7.3
harmonic rejection	Ni mirror	4.5° Ni mirror	4.5° monodetuned 50%
monochromator	Si(111)	Si(111)	Si(220)
energy range (eV)	8785−9731	8785−9731	8785−9731
energy resolution (eV)	1−2	1−2	0.5−1
upstream slit (mm)	1.2	1.2	1.2−1.0
hutch aperture slit (mm)	1.2−0.8	1.2−0.8	1.2−0.8
detector	13-element Ge	13-element Ge	13-element Ge
maximum count rate (kHz)	35	35	30
dead-time correction	No	No	No
number of scans	23	13	42
E_0 (start of EXAFS) (eV)	8985	8985	8985

EXAFS Measurements. EXAFS data were collected at the National Synchrotron Light Source (NSLS), Brookhaven National Laboratory, and at the Stanford Synchrotron Radiation Laboratory (SSRL). The Cl-containing and Cl-free data sets were collected at NSLS on beamline X9, whereas the high-pH sample was measured at SSRL. Experimental conditions are summarized in Table 1. The protein samples were measured as frozen glasses in 10% (v/v) (standard and Cl-free preparations) or 20% (v/v) (high-pH sample) glycerol at 11−14 K in fluorescence mode, using a 13-element Ge detector. To avoid detector saturation, the count rate of each detector channel was kept below 35 kHz by adjusting the hutch entrance slits or by moving the detector in or out from the cryostat windows. Under these conditions no dead-time correction was necessary. The summed data for each detector were then inspected, and only those channels that gave high-quality backgrounds free from glitches, dropouts, or scatter peaks were included in the final average. Raw data were averaged, background-subtracted, and normalized to the smoothly varying background atomic absorption using the EXAFS data reduction package EXAFSPAK (Graham George, 1990). The experimental energy threshold ($k = 0$) was chosen as 8985 eV. Care was taken to ensure that Zn impurities did not produce artifacts in the data at high k. A number of different background subtractions were carried out in which the data were truncated at different k values in the range $k = 12$−13.4 Å^{-1} energy to determine the value of k at which any contaminating Zn edge begins to affect

the data. For all three samples, the data correspond to the maximum k range that displays no perturbation from the presence of a zinc edge. It should also be noted that a tight energy window was used on the detector (0.2 V), such that >90% of any contaminating zinc fluorescence was windowed out of the data.

Data analysis was carried out by least-squares curve fitting, utilizing full curved-wave calculations as formulated by the SRS library program EXCURV (Binsted et al., 1988; Gurman, 1989; Gurman et al., 1984, 1986) by using methodology described in detail previously (Strange et al., 1987; Blackburn et al., 1991; Sanyal et al., 1993). The parameters refined in the fit were as follows: E_0, the photoelectron energy threshold; R_i, the distance from Cu to atom i; and $2\sigma_i^2$, the Debye–Waller term for atom i. For the protein fits, the coordination numbers were allowed to vary, but were constrained so as to produce Debye–Waller factors within reasonable limits (first shell, $0 < 2\sigma^2 < 0.012$; second shell, $0.005 < 2\sigma^2$). Multiple scattering contributions from outer shell (C_2, C_3, N_4, and C_5) atoms of coordinated histidine rings were simulated by using well-documented methodology described previously (Strange et al., 1987; Blackburn et al., 1991; Sanyal et al., 1993). The quality of the fits was determined by using a least-squares fitting parameter, F, defined as

$$F^2 = (1/N)\sum k^6(\chi_i^{\text{theor}} - \chi_i^{\text{exp}})^2 \qquad (2)$$

and referred to as the fit index.

RESULTS AND DISCUSSION

Chloride Depletion. Earlier EXAFS work on cytochrome *c* oxidase from bovine heart mitochondria indicated the presence of a heavy (second row) bridging S/Cl ligand between Fe_{a3} and Cu_B (Powers et al., 1979, 1981; Scott et al., 1986; Li et al., 1987). A more recent report (Powers et al., 1994) describing XAS of the Cu and Fe edges of the *B. subtilis* quinol oxidase cytochrome aa_3-600 likewise described evidence for a heavy bridging ligand. It has been considered that this ligand may be Cl rather than S (Li et al., 1987; Scott et al., 1988; Powers et al., 1994; see introduction). If substantiated, this would imply that either a substitution-labile or a tightly bound chloride ligand may be involved in bridging the two metals and mediating the magnetic coupling between them. We found that extensive dialysis of cytochrome aa_3-600, originally prepared in the presence of chloride, effectively removed Cl^- from the enzyme after 2–3 dialysis cycles. The concentration of Cl^- was <5 μM in the dialyzed 200–300 μM enzyme sample, both before and after denaturation by heat and acid (see Materials and Methods). We thus found no evidence for tightly and stoichiometrically bound chloride to cytochrome aa_3-600.

EXAFS of Cu_B. Three types of samples of fully oxidized cytochrome aa_3-600 were studied: (i) prepared by standard procedures (Lauraeus et al., 1991) with no precautions to eliminate chloride; (ii) identically prepared, but Cl-free samples (see earlier); and (iii), samples of normally prepared enzyme where the pH had been adjusted to 8.8 to diminish magnetic coupling between Fe_{a3} and Cu_B and, thus, to enhance the EPR signals from Cu_B (cf. Powers et al., 1994).

Figure 2 compares the background-subtracted raw EXAFS data for each of these three enzyme preparations. It can be seen that all three are extremely similar with respect to the main EXAFS features, particularly the standard enzyme and high-pH enzyme samples. The Fourier transforms (Figures 3–5) show a single intense peak at $r = 2.0$ Å (phase-corrected relative to the N phase shift) and smaller peaks at $r \sim 3.0$ and 4.0 Å, which are typical of coordinated histidine (Strange et al., 1987). Given the low metal concentration due to the low solubility of cytochrome aa_3-600 in aqueous environments, the signal to noise ratio is excellent. On the

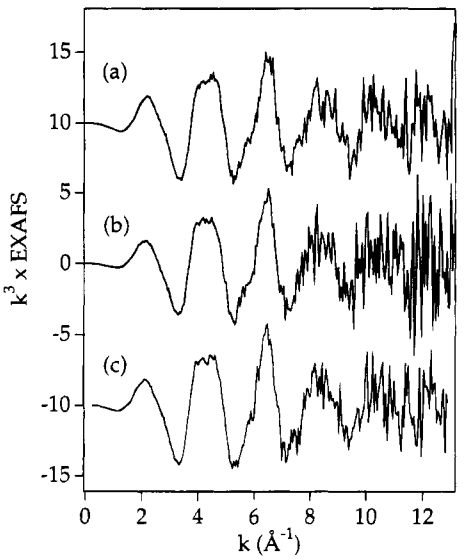

FIGURE 2: Comparison of the raw background-subtracted EXAFS of (a) standard enzyme preparation, (b) chloride-free enzyme, and (c) high-pH preparation. The data are plotted using 8985 eV corresponding to $k = 0$.

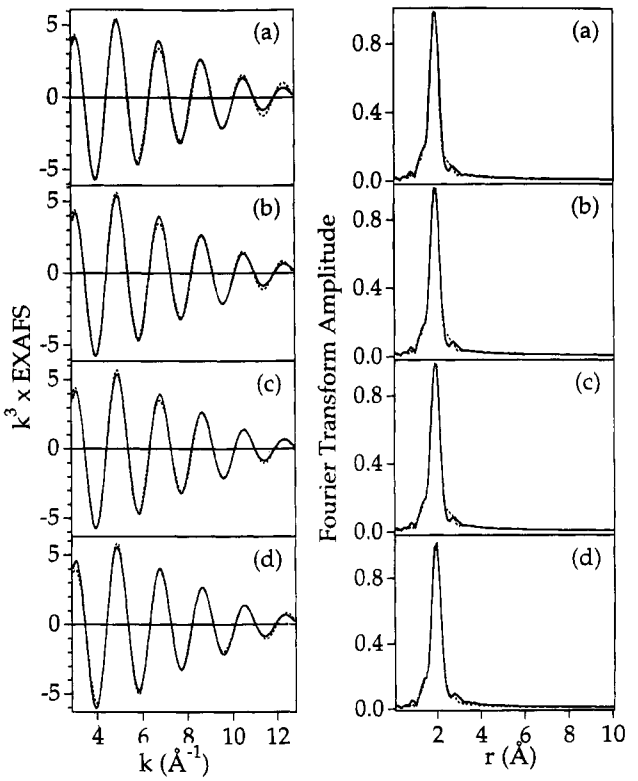

FIGURE 3: Analysis of first-shell Fourier-filtered data for standard enzyme preparation. Plots a–d correspond to fits A–D in Table 2. The Fourier filter window was $R = 0$–2 Å (uncorrected for the phase shift). Solid lines represent experimental data; dashed lines represent simulated data.

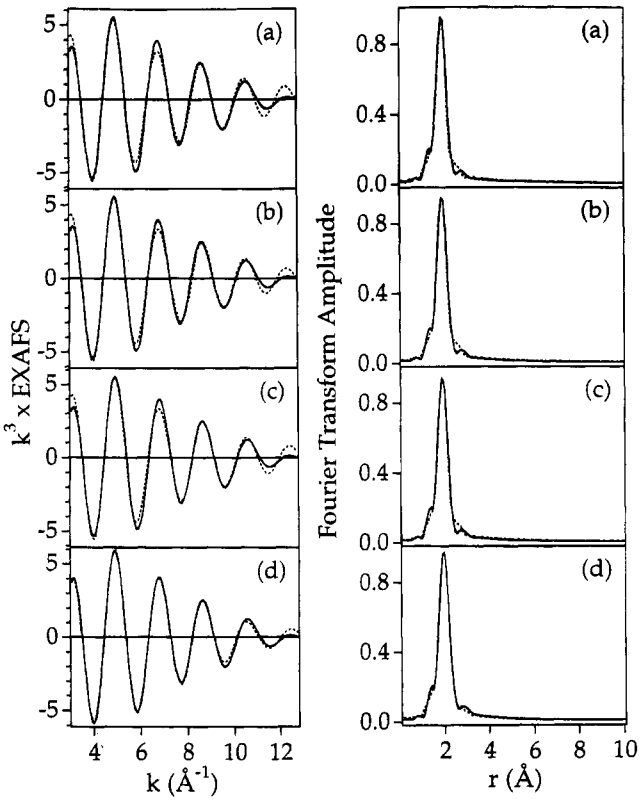

FIGURE 4: Analysis of first-shell Fourier-filtered data for the chloride-free enzyme. Plots a–d correspond to fits A–D in Table 2. The Fourier filter window was $R = 0-2$ Å (uncorrected for the phase shift). Solid lines represent experimental data; dashed lines represent simulated data.

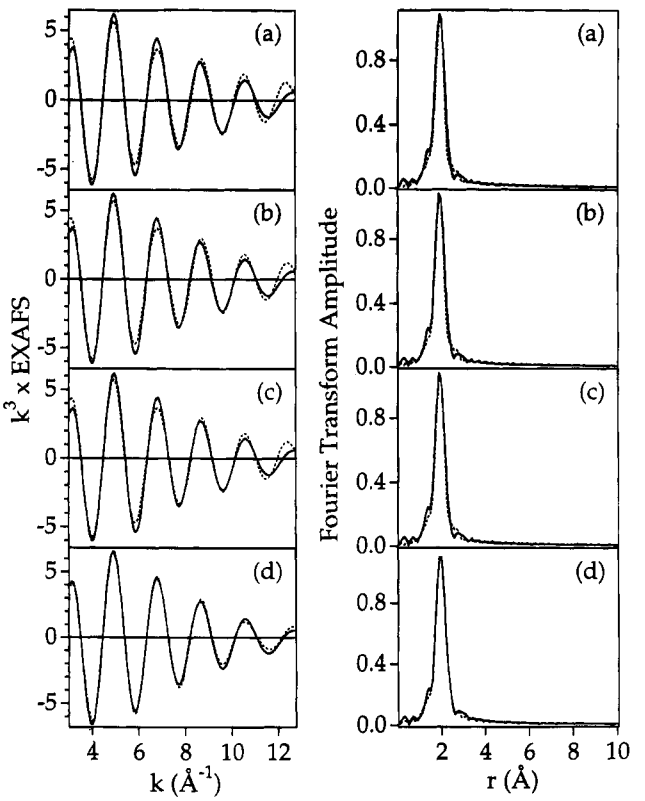

FIGURE 5: Analysis of first-shell Fourier-filtered data for the high-pH enzyme preparation. Plots a–d correspond to fits A–D in Table 2. The Fourier window was $R = 0-2$ Å (uncorrected for the phase shift). Solid lines represent experimental data; dashed lines represent simulated data.

other hand, the low concentrations impose a limit on the data range and, hence, on the resolution of the data. The distance resolution Δr is given by the expression, $\Delta r = \pi/2\Delta k$, and provides an estimate of the minimum splitting between shells of scatterers, which is obtainable from the data. Thus, for the present data extending between $k = 3$ and 12.5 Å^{-1}, we do not expect to resolve shells of scatterers separated by less than 0.12 Å. In addition, the presence of variable noise levels in each of the data sets above $k = 6$ Å^{-1} can introduce artifactual differences in Fourier-filtered first-shell data. Accordingly, we have been careful not to overinterpret the results from analyses of such data.

First-Shell EXAFS Data Analysis. Figures 3–5 show first-shell Fourier-filtered data for standard, Cl-free, and high-pH preparations. Initial analysis assumed no splitting of the first shell, and the data were simulated by four O/N scatterers using a single N phase shift. The results of these simulations are shown in Figures 3a, 4a, and 5a and Table 2. Simulations using a single shell of four low-Z scatterers give least-squares residuals (fit indexes, F) of 0.12, 0.27, and 0.45 for standard, Cl-free, and high-pH preparations, respectively. These fits are consistent with a tetragonal Cu_B site with y solvent ligands (H_2O, OH) and $4 - y$ histidine ligands in the equatorial plane. In this model, the rather large values of the Debye–Waller factors (0.008–0.010) may suggest a spread of distances within the first shell. Fits involving either three or five low-Z scatterers resulted in large increases in the value of F or unacceptably large Debye–Waller terms and were not investigated further. The signal to noise ratios for standard and high-pH samples are comparable and somewhat better than that of the Cl-free sample, but the value of F for the high-pH sample is 4 times that of the standard preparation. This difference in F between standard and high-pH preparations therefore may be significant. With this in mind, we have extended the analysis of first-shell data to

Table 2: Parameters Used in Fitting First-Shell Fourier-Filtered Data for the Standard, Chloride-Free, and High-pH Preparations of *Bacillus subtilis* Cytochrome aa_3-600[a]

fit	shell	distance	Debye–Waller (Å²)	E_0 (eV)	fit index
standard					
A	4 N/O	1.98	0.010	17.0	0.116
B	3 N/O	2.00	0.005	17.3	0.091
	1 N/O	1.90	0.002		
C	2 N/O	2.03	0.002	17.2	0.083
	2 N/O	1.92	0.003		
D	3 O/N	1.96	0.008	19.2	0.104
	1 S/Cl	2.16	0.021		
chloride-free					
A	4 N/O	1.98	0.010	18.5	0.287
B	3 N/O	2.01	0.007	18.6	0.222
	1 N/O	1.90	0.002		
C	2 N/O	2.05	0.005	17.7	0.278
	2 N/O	1.94	0.003		
D	3 N/O	1.95	0.009	21.5	0.080
	1 S/Cl	2.17	0.016		
high-pH					
A	4 N/O	1.97	0.008	18.4	0.446
B	3 N/O	2.00	0.008	18.0	0.400
	1 O/N	1.93	0.002		
C	2 N/O	2.03	0.005	17.7	0.380
	2 N/O	1.94	0.002		
D	3 N/O	1.94	0.006	21.1	0.088
	1 S/Cl	2.18	0.013		

[a] Estimated errors are ±0.002 for distances and ±25% for coordination numbers.

examine other combinations of scatterers.

Table 2 also contains results for modeling 3:1 N/O and 2:2 N/O split shells together with 3N:1S/Cl to test for the presence of a heavy atom scatterer. These calculations show that for the standard preparation a 3:1 split N/O shell with Cu−N/O bond lengths of 2.00 and 1.90 Å gives a comparable fit to the 4 N/O combination ($F = 0.091$). The splitting of the first-shell bond length, Δr, for this fit (0.1 Å) is at the limit of the resolution of the data. As expected, splitting the first shell results in lower Debye−Waller terms, with the lowest (0.002 Å^2) arising from the single O/N scatterer at 1.90 Å. This fit would be consistent with a Cu coordination sphere comprising three histidine ligands at 2.00 Å and an N/O donor ligand at 1.90 Å. This latter distance is more typical of an anionic ligand such as OH^- or phenolate. Since there is no significant increase in the value of F, the EXAFS analysis cannot distinguish between them. The 2:2 splitting of the N/O shell (Cu−N/O = 2.03, 1.92 Å) also gives a comparable value of F, although the Debye−Waller factors are smaller than anticipated for protein-bound scatterers (Blackburn et al., 1991).

The 3:1 and 2:2 fits are compared in Figures 3b,c, 4b,c, and 5b,c, for standard, Cl-free, and high-pH samples, respectively. The results for splitting the first shell into 3:1 and 2:2 N/O combinations are quantitatively similar for the Cl-free and high-pH samples (Table 2). Thus, in all cases a 3:1 N/O split is equally as good as the single-shell 4 N/O fit and results in three Cu−N/O interactions at 2.00 ± 0.02 Å and one Cu−N/O at 1.91 ± 0.02 Å. The 2:2 fit produces Cu−N/O distances of 2.04 and 1.94 ± 0.02 Å. Δr is ~0.1 Å in each case, which is at or just below the limit of resolution of the data. From this analysis we conclude that there are four first-shell (equatorial) O/N ligands, at least one of which could be either a water molecule or an anionic ligand such as OH^- or tyrosinate.

The preceding analysis shows that a different composition of N/O first-shell ligands or distances is not the origin of the large increase in the value of F between standard and high-pH samples. It also cannot be attributed to signal to noise artifacts since S/N are comparable for standard and high-pH samples and less than for the Cl-free sample, whereas the F values for the fits of the Cl-free sample are smaller than those for the high-pH data. One possibility is the presence of variable amounts of coordinated Cl^- in the standard and high-pH preparations. To investigate this possibility, we have carried out 3N:1S/Cl fits to the data. These are shown in Table 2 as fits D, as well as in Figures 3d, 4d, and 5d. For the standard preparation the data will tolerate S/Cl at 2.18 Å, but with a very large Debye−Waller term (0.021 Å^2) and a moderate increase in F. The Debye−Waller term for the S/Cl shell is almost an order of magnitude greater than that expected for a single first-shell scatterer, especially as the bond length is short for Cu−Cl (see Powers et al., 1994). For example, the single coordinated S from methionine at the Cu_B site of dopamine-β-monooxygenase (Reedy & Blackburn, 1994) has a Debye−Waller term of 0.003−0.004. We conclude that Cl is not present as a major component in the standard preparation.

However, the same analysis applied to the high-pH data yields quite different results. Inclusion of an S/Cl wave at 2.18 Å leads to a dramatic decrease in F from 0.45 to 0.09, with a Debye−Waller term of 0.013. While the latter is large for a first-shell Debye−Waller term, the improvement in the fit suggests that some Cl^- may be coordinated to a vacant coordination position at Cu_B. When the Debye−Waller factor for the S/Cl shell is fixed at 0.005 Å^2 (estimated to be within the range of acceptable values for a single shell at 10−20 K) and the coordination numbers are refined, a value of 3.4 N/O at 1.94 Å and 0.5 Cl^- ligands at 2.18 Å is obtained. These results may suggest that a substitution-labile exogenous ligand-binding site is present on Cu_B, which can coordinate Cl^-, and is fractionally occupied in some preparations of cytochrome aa_3-600. However, this conclusion should be treated with caution for three reasons: (i) inclusion of the S/Cl component improves the simulation of the Cl-free data almost as well as for the high-pH sample; (ii) the Cu−N and Cu−Cl bond lengths of 1.94 and 2.18 Å, respectively, are anomalously low for a four-coordinate Cu(II) species; and (iii) the 3N/O:1S/Cl model leads to very poor fits when the multiple scattering due to the histidine ligands is included and the unfiltered raw data are simulated (see the following).

Multiple Scattering EXAFS Analysis and Histidine Coordination. The second- and third-shell carbon and nitrogen atoms of the imidazole rings of histidine ligands contribute strongly to the EXAFS of metal−histidine systems, because the ring geometry is approximately fixed and the motion of the ring atoms is therefore correlated with the first-shell metal−nitrogen vibrations in a coherent way. In addition, the Cu−N_1−C_3 and Cu−N_1−N_4 angles are 163°, which introduces strong multiple scattering effects due to this nearly collinear arrangement of atoms. Previous studies on Cu−histidine-containing metalloproteins (Blackburn et al., 1987, 1991, 1992) and model compounds (Strange et al., 1987; Blackburn et al., 1988; Sanyal et al., 1993) have shown that these multiple scattering effects can be well-simulated and can provide an estimate of the number of coordinated histidine ligands in favorable cases. We have carried out similar calculations on the EXAFS of Cu_B of cytochrome aa_3-600 in an attempt to obtain an estimate of histidine coordination number. These simulations are based on the 4 N/O first-shell fits since splitting of the first shell did not improve the fit index significantly. Thus, the simulations include scattering contributions from y imidazole rings with Cu−N(imid) = 1.98 Å and $(4 - y)$ additional N/O shells at 1.98 Å. The results for the standard and high-pH preparations are shown in Figures 6 and 7, respectively. Acceptable fits are obtained for either two or three histidine ligands, the differences being exclusively due to differences in outer-shell Debye−Waller factors. In metalloprotein systems it is difficult to predict the magnitude of the outer shell Debye−Waller terms, as they depend on the spread of the average Cu−N(his) distances in the first shell. The two-histidine fit is intuitively less satisfactory as the Debye−Waller terms for the second shell (Table 3) are almost identical to those for the first shell (0.01 Å^2) and are smaller than what we generally observe. On the other hand, values more representative of other Cu−his metalloprotein systems (0.015 and 0.025 Å^2 for shells two and three, respectively) are obtained in the three-histidine fit. We conclude that the most likely coordination for Cu_B is three histidine ligands at 1.98 ± 0.02 Å and either a water molecule at 1.98 ± 0.02Å, or an anionic ligand (OH^-, phenolate) at 1.90 ± 0.02 Å. However, these EXAFS data cannot exclude a 2-histidine, 2-O/N donor structure.

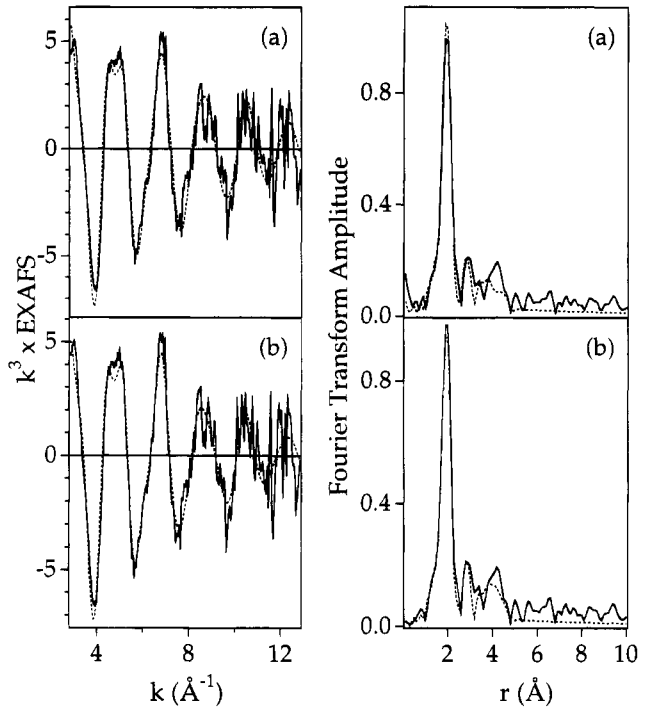

FIGURE 6: Simulation of the unfiltered EXAFS of the standard enzyme preparation, including multiple scattering contributions from imidazole rings of histidine ligands: (a) three-histidine fit; (b) two-histidine fit. Parameters used in the simulation are given in Table 3.

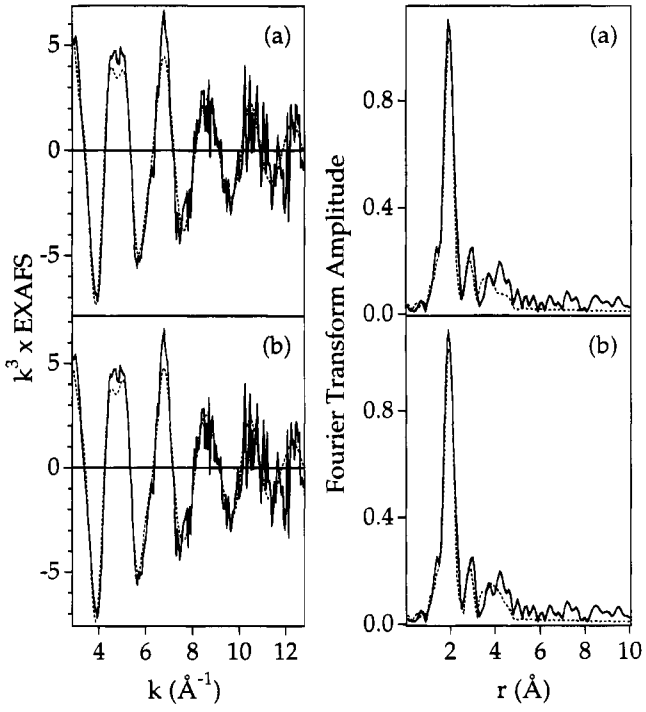

FIGURE 7: Simulation of the unfiltered EXAFS of the high-pH enzyme preparation, including multiple scattering contributions from imidazole rings of histidine ligands: (a) three-histidine fit; (b) two-histidine fit. Parameters used in the simulation are given in Table 3.

Copper−Iron Interaction. The Fourier transforms shown in Figure 2 show no evidence of intense outer shell peaks due to an Fe−Cu interaction, and the outer shell peaks that are seen can be simulated by imidazole C/N multiple scattering interactions. Inclusion of a Cu−Fe interaction led to a small improvement in the fit index, with a Cu−Fe distance of 3.32 ± 0.05 Å in both standard and high-pH samples. However, inclusion of 2C at a similar distance produced the same improvement, and the evidence for Cu−Fe therefore must be considered speculative. Model studies in two independent laboratories have examined oxo-, hydroxo-, and cyano-bridged (porphyrin)iron(III)−copper(II) complexes in order to probe likely models of Fe−Cu bridging in heme−copper oxidases (Nanthakumar et al., 1993; Scott et al., 1994; Lee & Holm, 1993; Karlin et al., 1994). Oxo-bridged species show nearly linear Cu−O−Fe units, the EXAFS of which shows extremely intense outer shell peaks in the Fourier transforms due to a strong multiple scattering interaction (Scott et al., 1995; Fox et al., 1995). The oxo-group can be protonated to give hydroxo-bridged species in which the Cu−O−Fe angle has decreased to 157°, such that multiple scattering is no longer observable. A weaker Cu−Fe interaction is observed in the hydroxo-bridged model complex. Application of these models to the cytochrome aa_3-600 system allows oxo bridging between Fe and Cu to be unambiguously ruled out, since there is no evidence for an analogous Cu−O−Fe collinear interaction. On the other hand, a hydroxo-bridged Cu−OH−Fe structure remains a possibility.

Table 3: Parameters Used in the Simulation of Unfiltered Cu-K-EXAFS of Cytochrome aa_3-600, Including Multiple Scattering Contributions from Outer Shell Atoms of the Imidazole Rings[a]

first-shell coordination			imidazole ring geometry[b]			
shell	distance (Å)	DW (Å^2)	shell	distance (Å^2)	DW (Å^2)	angle (deg)
3 His	1.98	0.008[c]	Cu−N1	1.98	0.008[c]	
1 O/N	1.98	0.008[c]	Cu−C2	2.83	0.015	127
			Cu−C5	2.94	0.015	−127
			Cu−C3	4.03	0.025	163
			Cu−N4	4.23	0.025	−163
2 His	1.98	0.008[c]	Cu−N1	1.98	0.008[c]	
2 O/N	1.98	0.008[c]	Cu−C2	2.83	0.010	127
			Cu−C5	2.94	0.010	−127
			Cu−C3	4.03	0.017	163
			Cu−N4	4.23	0.017	−163

[a] Identical simulations were used for both standard and high-pH preparations, except for first-shell Debye−Waller terms and E_0 (see footnote *c*). [b] The atom numbering scheme and definitions of angles are as given in Blackburn et al. (1991). [c] The values of the first-shell DW terms given in the table are for the high-pH sample. The DW term for the standard sample was 0.010. E_0 values were 16.8 and 18.0 eV for standard and high-pH samples, respectively.

EPR of Cytochrome aa_3-600 at High pH. The EPR spectrum of the high-pH cytochrome aa_3-600 sample at liquid helium temperature is like the reported X-band spectrum at 12 K (Powers et al., 1994), in that it exhibits signals from the high-spin ferric Fe_{a3} ($g_\perp = 6$, $g_\parallel = 2$) and the low-spin ferric Fe_a ($g = 3.07, 2.25, 1.45$), as well as from cupric Cu_B (Figure 8A). In addition, a signal emerges at $g = 2.65$ that is similar to that previously attributed to low-spin ferric Fe_{a3}−OH^- (Wilson et al., 1976; Shaw et al., 1978; Lanne et al., 1979). The EPR signal of Cu_B was shown in the X-band studies to exhibit an axial signal with $g_\perp = 2.05$, $g_\parallel \sim 2.23$, and resolved Cu hyperfine splittings with $A_\parallel \sim 420$ MHz (cf. Powers et al., 1994). At 35 GHz the $g_\perp$ feature of Cu_B is clearly resolved, but the $g_\parallel$ region is not well-defined because of overlap with the $g = 2.25$ feature of low-spin Fe_a, and perhaps because of g strain as well (Figure 8B). In fact, the EPR spectrum of Cu_B totally overlaps the EPR

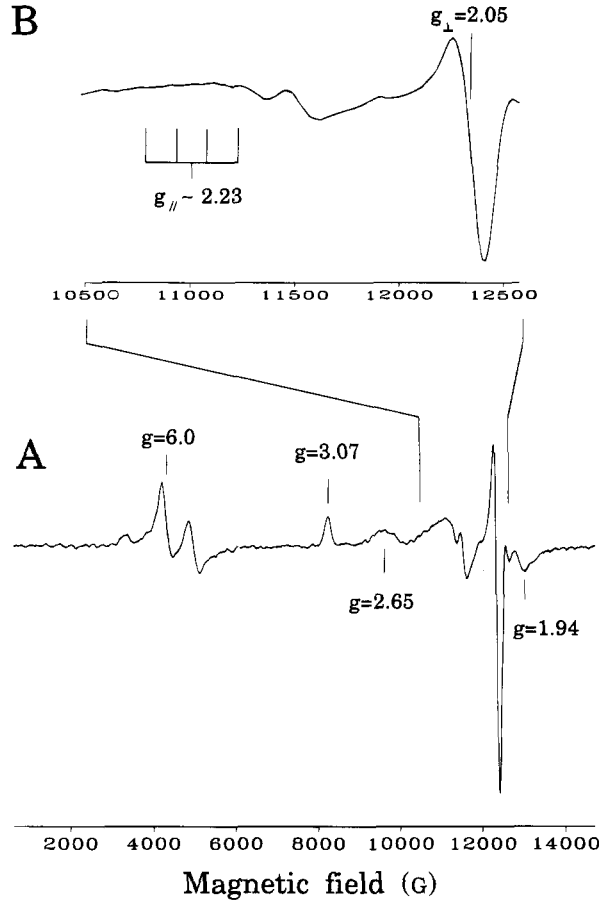

FIGURE 8: Continuous-wave 35 GHz EPR spectra of cytochrome aa_3-600 at pH 8.8: (A) broad-scan spectrum; (B) enlargement of Cu_B region. The positions expected for the Cu hyperfine features at $g_{||}$ are indicated, viz., four lines centered at $g_{||}$ and separated by $A_{||} \sim 150$ G. Experimental conditions: microwave power, 0.2 mW; modulation amplitude, 2 G; temperature, 2 K.

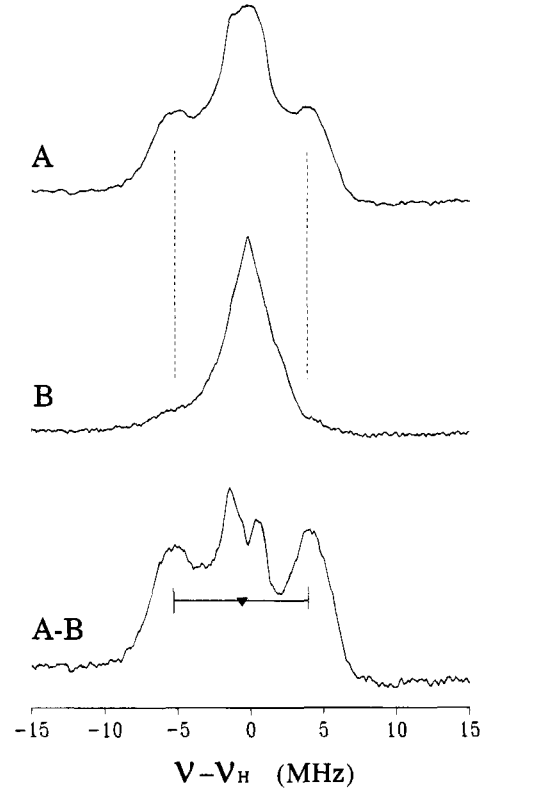

FIGURE 9: Continuous-wave 35 GHz ^1H ENDOR spectra for cytochrome aa_3-600 taken at $g_\perp = 2.05$ in (A) H_2O buffer, (B) ^2H_2O buffer, and (A−B) the difference spectrum between (A) and (B), showing a hyperfine-split doublet centered at the proton Larmor frequency (~52.2 MHz) corresponding to an exchangeable proton. Experimental conditions: modulation amplitude, 0.6 G; RF scan rate, 1.0 MHz/s, 50 scans; magnetic field (B_o), (A) 12 250 G, (B) 12 290 G; temperature, 2 K.

spectra of the hemes (Figure 8A). However, in the ENDOR experiments described in the following, it was straightforward to ascertain whether a peak in the spectrum obtained at a field within the Cu_B EPR envelope is associated with this center or with heme; a peak associated with Cu_B disappears at fields outside the EPR envelope of this center.

^1H ENDOR Results and Analysis. The ^1H ENDOR spectrum for cytochrome aa_3-600 in aqueous buffer taken at $g = 2.05$ (Figure 9A) shows a peak at ν_H and a doublet from a strongly coupled proton with a hyperfine coupling constant, $A_{||} \sim 10$ MHz. This proton is associated with the Cu_B site because the doublet is absent when the field is set outside the Cu_B EPR envelope (data not shown). The proton is exchangeable, as shown by its loss in ^2H_2O buffer (Figure 9B). Its presence was further confirmed by preliminary ^2H pulsed ENDOR experiments: a spectrum taken at the same g value showed that the deuteron introduced by the exchange has the corresponding ^2H hyperfine coupling constant, $A(^2H) = 1.54$ MHz [$|A(^1H)/A(^2H)| = |\nu(^1H)/\nu(^2H)| = 6.51$].

The proton hyperfine coupling constant of 10 MHz is reasonable for a H_xO ligand (in this case possibly a hydroxide, see the following) coordinated to the copper, as shown previously by Atherton and Horsewill (1979) for the $Cu(H_2O)_6^{2+}$ complex. The H/D difference spectrum (Figure 9, bottom trace) also appears to show an additional weakly ^1H-coupled doublet [$A(^1H) \sim 2.2$ MHz]. However, for frequencies so near to ν_H, changes upon H/D exchange cannot be reliably assessed in CW spectra because of possible changes in the distant ENDOR response from solvent. To prove whether or not this difference is associated with an exchangeable local proton requires additional ^1H and ^2H pulsed ENDOR studies.

^{14}N ENDOR Results and Analysis. Figure 10 shows selections from a series of ENDOR spectra taken across the Cu_B EPR envelope. The spectra shown were taken from $g = 2.23 \sim g_{||}$ to $g = 2.02 < g_\perp$ and display the resonance frequency range expected for a ^{14}N ligand to copper. The spectrum at $g = 2.23$ is single-crystal-like for Cu_B, arising from molecules with the external field lying along $g_{||}$, and each ^{14}N ligand to Cu should give one pattern as described by eq 1 (see Materials and Methods; Hoffman et al., 1993). As shown in the figure, the three peaks with $\nu > 10$ MHz (labeled as *a*, *b*, and *c*) can be assigned to ν_+ features of three ^{14}N ligands to a metal ion, each without further resolved quadrupole splittings. The peaks disappear at fields outside the Cu_B EPR envelope (e.g., at $g = 2.02$; Figure 10), and thus they are associated with Cu_B. No pair of these three ^{14}N peaks is separated by $2\nu(^{14}N)$, as would be required for a ν_+,ν_- pair from ^{14}N. In particular, peaks a and b cannot be $\nu_+,_-$ Larmor-split partners because they are separated by less than $2\nu(^{14}N)$ and peak b is more intense than a, whereas a ^{14}N ν_- feature normally is substantially lower in intensity than the corresponding ν_+ and may indeed be missing entirely. In addition, the peak separations are too great for any two adjacent peaks to be assigned as a quadrupole split $\nu_+(\pm)$ pair from a single ^{14}N. For example, the separations

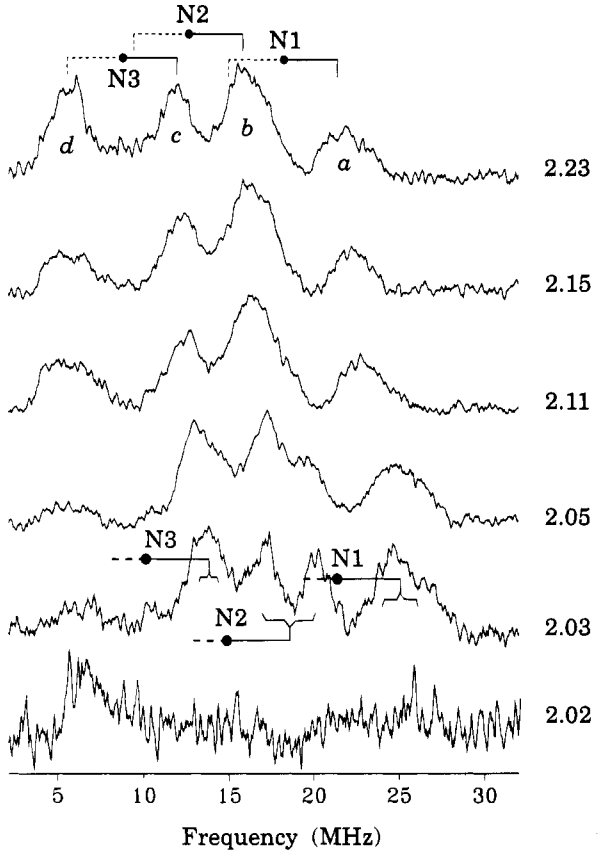

FIGURE 10: Field dependence of Cu_B ^{14}N ENDOR spectra taken at indicated g values across the EPR envelope of Cu_B. Experimental conditions: microwave frequency, 35.2 GHz; modulation amplitude, 1.25 G; RF scan rate, 2 MHz/s; temperature, 2 K. Fields from the top: 11 277, 11 696, 11 917, 12 266, 12 387, and 12 448 G. Temperature was 2 K; each spectrum required about 1−2 h of signal averaging.

between peaks a and b and between b and c are 7 and 5 MHz, respectively, which are much greater than the maximum possible quadrupole splitting for Cu-bound nitrogenous ligands of ca. 3.5 MHz (Gurbiel et al., 1993). Thus, a−c must be unresolved ν_+ branches of three distinct ^{14}N ligands of Cu_B. The fourth peak, d, arises from the heme pyrrole ^{14}N of the low-spin Fe_a, as predicted from earlier ENDOR studies (Mulks et al., 1979) and as confirmed by its persistence at fields outside the Cu_B EPR envelope (see, for example, the $g = 2.02$ trace in Figure 10). No peaks from heme are expected in the range $\nu > 10$ MHz, and indeed none are seen outside the Cu_B EPR envelope (Figure 10, $g = 2.02$). Thus, the Q-band ENDOR spectra disclose three distinct ^{14}N ligands of Cu_B. At $g_{\|}$ their hyperfine couplings are $A(N_1) = 37$ MHz, $A(N_2) = 25$ MHz, and $A(N_3) = 17$ MHz, with peaks a, b, and c corresponding to ligands 1, 2, and 3.

As the field is increased from $g_{\|}$ to $g_\perp = 2.05$, the $\nu_+(N_1)$ peak shifts to higher frequency as the result of hyperfine anisotropy; at $g_\perp$, $A(N_1) \sim 42$ MHz. The peak for N_3 does likewise, but to a lesser extent; at $g_\perp$, $A(N_3) \sim 20$ MHz. The peak from N_2 splits with increasing field, with one feature remaining at $\nu \sim 17$ MHz and the other shifting to $\nu \sim 20$ MHz at $g = 2.03$. This pattern could arise solely from hyperfine anisotropy and is consistent with an axial hyperfine tensor with $A_{\|}(N_2) \sim 31$ MHz normal to $g_{\|}$, and $A_\perp(N_2) \sim 25$ MHz. However, it is also possible that the splitting at $g_\perp$ arises from quadrupole interactions (e.g., as in the Cu_A center; Gurbiel et al., 1993). This issue would require ^{15}N labeling to be resolved, but is not important for ligand assignment. The hyperfine coupling constants of the three ^{14}N ligands of Cu_B in cytochrome aa_3-600 are quite similar to those reported by Cline et al. (1983) for Cu_B in an oxygen intermediate state of mitochondrial cytochrome c oxidase, for type 3 copper in laccase, or for those observed by ENDOR for Cu_B in cytochrome ba_3 (Surerus et al., 1992), as summarized in Table 4. In the last case, resolved features in the EPR spectrum suggested that Cu_B has four histidine ligands and that one of the ^{14}N ENDOR signals, therefore, reflected two unresolved nitrogens. However, in the present case such a situation is contradicted by the proton ENDOR, which shows one of the four coordination sites to be occupied by H_xO.

Table 4: ^{14}N Hyperfine Coupling Constants of Cu_B in Cytochrome aa_3-600 in Comparison to Those of Other Cu Complexes[a]

	N_1 (MHz)	N_2 (MHz)	N_3 (MHz)
Cu_B			
cytochrome aa_3-600[b]	42, 37	31, 25	20, 17
oxygen intermediate of cytochrome c oxidase (beef heart)[c]	40	35	28
cytochrome ba_3[d]	37	32	28
laccase, type 3 copper[b]	50, 40	45, 36	36, 30
blue copper (type 1)[e]	44−50	19−23	
$Cu(imidazole)_4^{2+}$	41[f]		

[a] Uncertainty: $A \pm 2$ MHz; quadrupole interactions are not resolved. [b] First value was measured at $g_\perp$ and the second at $g_{\|}$. [c] Measured at $g_\perp$. [d] See Surerus et al. (1993). [e] Hyperfine couplings are roughly isotropic; the range is given (Roberts, 1982; Werst et al., 1991). [f] The hyperfine couplings are roughly isotropic (van Camp et al., 1981).

The differences among the three Cu_B ligands indicate low symmetry at the Cu_B site. The hyperfine coupling values for N_1 are essentially the same as those for $Cu(Im)_4^+$, which suggests a normal Cu−N bond directed along the lobe of the $d_{x_2-y_2}$ orbital; larger couplings are sometimes seen for N_1 in blue copper (Table 4). The values for N_3 are comparable to those for the second ^{14}N His of blue copper, while N_2 has intermediate values. The three nitrogen ligands of Cu_B here have slightly smaller couplings than the corresponding ligands in laccase; N_1 and N_2 have couplings comparable to those of Cu_B of the oxygen intermediate of bovine heart cytochrome c oxidase and in cytochrome ba_3, while that for N_3 appears smaller.

The ^1H and ^{14}N ENDOR data taken together thus establish a 3N:1O coordination sphere for Cu_B in the high-pH binuclear center. In conjunction with the EXAFS data, this shows the coordination to be 3His:1O and rules out 2His:2O. The difference in hyperfine couplings among the three Cu_B histidine ligands suggests that Cu_B does not exhibit a simple square-planar geometry with all four ligands lying in a plane along the $x-y$ axes. In such a case one would expect the coupling constants to be much more similar, with two being more or less the same by symmetry. The blue copper proteins are examples where substantially different hyperfine couplings are exhibited by two histidyl ligands that form part of a trigonal arrangement about Cu and do not have equal overlap with the lobes of the odd-electron $d_{x_2-y_2}$ orbital on copper (Werst et al., 1991).

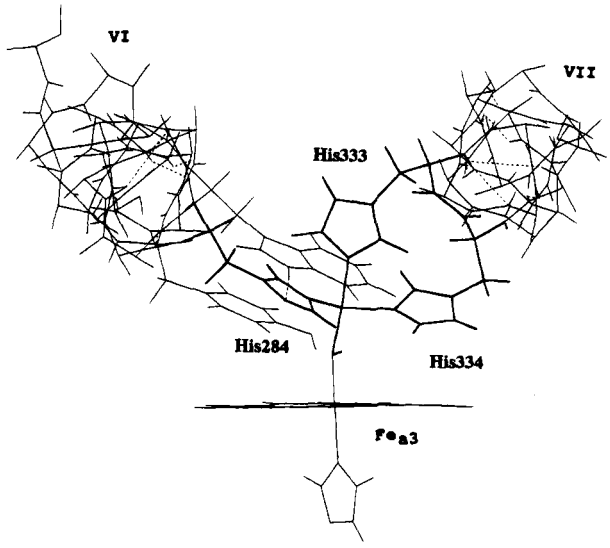

FIGURE 11: Structural model of the binuclear center.[2] The structure is viewed in the plane of heme a_3 (roughly perpendicular to the membrane), showing helixes VI and VII. The Cu_B site is highlighted and shown with its three histidine ligands and one OH^- ligand, which forms a bridge to Fe_{a3}. A conserved tryptophan residue (Trp280) is shown above the Cu_B site (toward the viewer) and is close enough to form a hydrogen bond to the $\delta 1$ nitrogen of His284. A conserved tyrosine (Tyr288), which may ligate Cu_B in some states of the catalytic cycle, is shown below the Cu_B site (see the text). The model was built and energy-minimized by using the HyperChem program (release 2, Autodesk Inc.) and the MM+ force field. Bond lengths from the present work (see text) were used as restraints in the minimization.

CONCLUSIONS AND STRUCTURAL ASSIGNMENTS

The consistency between the ENDOR and EXAFS results is remarkable: Cu_B in the oxidized cytochrome aa_3-600 is in a site of low symmetry, with three inequivalent histidine ligands at 1.98 (±0.02) Å and a fourth oxygenous ligand with (an) exchangeable proton(s) at the same distance if H_2O or at 1.90 (±0.02) Å if OH^- or tyrosinate. Figure 11 shows a model of the binuclear center where these structural features have been incorporated. Our results establish the structure and coordination of Cu_B(II) as being similar to either one of the two type 3 copper ions of ascorbate oxidase (and laccase; Messerschmidt et al., 1989), as supported by the similar histidine hyperfine coupling constants (Table 4; cf. Cline et al., 1983).

Most importantly, this study establishes that the enzyme does not bind Cl^- tightly and that Cl^- present in excess in the isolation medium can be effectively removed by dialysis. Moreover, the Cu EXAFS shows no significant S/Cl bridging ligand coordinated to Cu_B. Some indications of a subpopulation of enzyme that might in some conditions coordinate Cl^- to an exchangeable coordination site were found, which might explain the difference from earlier studies where a heavy bridging ligand between Fe_{a3} and Cu_B has been consistently reported (see Introduction).

The identity of the three histidines that ligate Cu_B seems clear on the basis of the primary structure alignment of over 80 heme−copper oxidases (Calhoun et al., 1994), identifying six fully conserved histidines, and site-directed mutagenesis of these histidines combined with spectroscopic work (see introduction). On this basis, the adjacent His333 and His334, located in the putative transmembrane helix VII of subunit I, have already been strongly implicated as ligands of Cu_B [see Hosler et al. (1993) for a review]; their mutation most likely leads to loss of the Cu_B from the enzyme (Minagawa et al., 1992; Brown et al., 1994). The invariant histidine, His284, is located in the putative transmembrane helix VI. Its mutation has suggested coordination to Cu_B (Hosler et al., 1993), but in this case the metal may well remain bound to the site, as judged from CO recombination kinetics experiments (Brown et al., 1994). Hence, H284 appears structurally inequivalent to H333 and H334 with respect to coordination to Cu_B. It should be emphasized that most of the evidence from site-directed mutagenesis on specific histidine coordination to Cu_B has relied on spectroscopic studies on enzyme where the copper is reduced, while the present study has focused on oxidized Cu_B. We conclude that the three inequivalent Cu_B ligand histidines observed here in the oxidized state of cytochrome aa_3-600 are most probably H284 in helix VI and H333 and H334 in helix VII (see Figure 11).[2]

Our EXAFS data exclude an oxo bridge between Fe_{a3} and Cu_B in oxidized cytochrome aa_3-600, but would be consistent with a hydroxide or a phenolate (tyrosinate) bridge. On the other hand, the EXAFS of the standard and high-pH samples was virtually the same even though the magnetic Fe_{a3}−Cu_B coupling was considerably weakened in the latter case, causing the development of the EPR signal of Cu_B, which was a prerequisite for the ENDOR analysis. Thus, it might be the bond between Fe_{a3} and a bridging XOH ligand at neutral pH that breaks at high pH, with XOH remaining bound to Cu_B at a similar bond length. The high-pH-induced break of the magnetic coupling could be brought about by OH^- attack on the bridge, followed by OH^- binding to the sixth axial position of Fe_{a3}. The generation of a low-spin ferric Fe_{a3} species ($g = 2.65$ signal; see Figure 8) at high pH has been interpreted as Fe_{a3}^{3+}−OH^- (Wilson et al., 1976; Shaw et al., 1978; Lanne et al., 1979), in agreement with this possibility.

The fact that our ENDOR study showed the oxygenous Cu_B ligand to have an exchangeable proton would *a priori* tend to favor OH^- over tyrosine as the ligand. An EPR study using ^{17}O-enriched O_2 established that Cu_B has an ^{17}O-labeled oxygenous ligand, probably OH^-, in an intermediate state of the catalytic cycle (Hansson et al., 1982). This emphasizes the ability of Cu_B to coordinate OH^- derived from the dioxygen chemistry in the binuclear site. A highly conserved tyrosine in helix VI (Y288) is predicted to lie one helical turn below and on the same helical face as H284 (Figure 11). Mutagenesis of Y288 yields phenotypes similar to those following mutation of H284, which also supports at least a close connection to the Cu_B site. Consequently, Y288 has been proposed to be a fourth ligand of Cu_B (Thomas et al., 1994), and thus a tyrosinate bridge between Fe_{a3} and Cu_B should be considered as well. While a protonated tyrosine could hardly be able to bridge Fe_{a3}^{3+} and Cu_B^{2+}, it should be recalled that our ENDOR data were aquired after breaking the magnetic coupling, and hence presumably the bridge, at high pH. On the other hand, it is somewhat difficult to accept that a protonated tyrosine would ligate Cu_B at pH 8.8, and we therefore favor OH^- as the more plausible Cu_B ligand in these conditions. However, as seen in the structural model of Figure 11, Y288 can indeed come very close to the Cu_B site and might substitute for OH^- as a Cu_B ligand in some states of the catalytic cycle.

REFERENCES

Atherton, N. M., & Horsewill, A. J. (1979) *Mol. Phys. 37*, 1349−1361.

Babcock, G. T., & Wikström, M. (1992) *Nature 356*, 301−309.

Binsted, N., Gurman, S. J., & Campbell, J. W. (1988) *Daresbury Laboratory EXCURV88 Program.*

Blackburn, N. J., Strange, R. W., McFadden, L.-M., & Hasnain, S. S. (1987) *J. Am. Chem. Soc. 109*, 7162−7170.

Blackburn, N. J., Strange, R. W., Farooq, A., Haka, M. S., & Karlin, K. D. (1988) *J. Am. Chem. Soc. 110*, 4263−4272.

Blackburn, N. J., Hasnain, S. S., Pettingill, T. M., & Strange, R. W. (1991) *J. Biol. Chem. 266*, 23120−23127.

Blackburn, N. J., Strange, R. W., Carr, R. T., & Bencovic, S. J. (1992) *Biochemistry 31*, 5298−5303.

Brown, S., Rumbley, J. N., Moody, A. J., Thomas, J. W., Gennis, R. B., & Rich, P. R. (1994) *Biochim. Biophys. Acta 1183*, 521−532.

Calhoun, M. W., Thomas, J. W., & Gennis, R. B. (1994) *Trends Biochem. Sci. 19*, 325−330.

Chance, B., & Powers, L. (1985) *Curr. Top. Bioenerg. 14*, 1−19.

Cline, J., Reinhammar, B., Jensen, P., Venters, R., & Hoffman, B. M. (1983) *J. Biol. Chem. 258*, 5124−5128.

Fox, S., Nanthakumar, A., Wikström, M., Karlin, K. D., & Blackburn, N. J. (1995) *J. Am. Chem. Soc.* (submitted for publication).

Gurbiel, R. J., Fann, Y. C., Surerus, K. K., Werst, M. M., Musser, S. M., Doan, P. E., Chan, S. I., Fee, J. A., & Hoffman, B. M. (1993) *J. Am. Chem. Soc. 115*, 10888−10894.

Gurman, S. J. (1989) in *Synchrotron Radiation and Biophysics* (Hasnain, S. S., Ed.) pp 9−42, Ellis Horwood Ltd., Chichester, United Kingdom.

Gurman, S. J., Binsted, N., & Ross, I. (1984) *J. Phys. C 17*, 143−151.

Gurman, S. J., Binsted, N., & Ross, I. (1986) *J. Phys. C 19*, 1845−1861.

Hansson, Ö., Karlsson, B., Aasa, R., Vänngård, T., & Malmström, B. G. (1982) *EMBO J. 1*, 1295−1297.

Hoffman, B. M., DeRose, V. J., Doan, P. E., Guriel, R. J., Houseman, A. L. P., Telser, J. (1993) *Biological Magnetic Resonance* (Berliner, L. J., & Reuben, J., Eds.) Vol. 13, pp 151−218, Plenum Press, New York.

Hoffman, B. M., DeRose, V. J., Ong, J. L., & Davoust, C. E. (1994) *J. Magn. reson. Ser. A 110*, 52−57.

Hosler, J. P., Ferguson-Miller, S., Calhoun, M. W., Thomas, J. W., Hill, J., Lemieux, L., Ma, J., Georgiou, C., Fetter, J., Shapleigh, J., Tecklenburg, M. M. J., Babcock, G. T., & Gennis, R. B. (1993) *J. Bioenerg. Biomembr. 25*, 121−136.

Karlin, K. D., Nanthakumar, A., Fox, S., Murthy, N. N., Ravi, N., Huynh, B. H., Orosz, R. D., & Day, E. P. (1994) *J. Am. Chem. Soc. 116*, 4753−4763.

Karlsson, B., Aasa, R., Vänngård, T., & Malmström, B. G. (1981) *FEBS Lett. 131*, 186−188.

Lanne, B., Malmström, B. G., & Vänngård, T. (1979) *Biochim. Biophys. Acta 545*, 205−214.

Lappalainen, P., Aasa, R., Malmström, B. G., & Saraste, M. (1993) *J. Biol. Chem. 268*, 26416−26421.

Lauraeus, M., Haltia, T., Saraste, M., & Wikström, M. (1991) *Eur. J. Biochem. 197*, 699−705.

Lauraeus, M., Wikström, M., Varotsis, C., Tecklenburg, M. M. J., & Babcock, G. T. (1992) *Biochemistry 31*, 10054−10060.

Lee, S. C., & Holm, R. H. (1993) *J. Am. Chem. Soc. 115*, 11789−11798.

Li, P. M., Gelles, J., Chan, S. I., Sullivan, R. J., & Scott, R. A. (1987) *Biochemistry 26*, 2091−2095.

Messerschmidt, A., Rossi, A., Ladenstein, R., Huber, R., Bolognesi, M., Gatti, G., Marchesini, A., Petruzzelli, R., & Finazzi-Agró, A. (1989) *J. Mol. Biol. 206*, 513−529.

Minagawa, J., Mogi, T., Gennis, R. B., & Anraku, Y. (1992) *J. Biol. Chem. 267*, 2096−2104.

Minghetti, K. C., Goswitz, V. C., Gabriel, N. E., Hill, J. J., Barassi, C. A., Georgiou, C. D., Chan, S. I., & Gennis, R. B. (1992) *Biochemistry 31*, 6917−6924.

Mitchell, P. (1987) *FEBS Lett. 222*, 235−245.

Mitchell, P. (1988) *Ann. N.Y. Acad. Sci. 550*, 185−198.

Morgan, J. E., Verkhovsky, M. I., & Wikström, M. (1994) *J. Bioenerg. Biomembr. 26*, 599−608.

Mulks, C. F., Scholes, C. P., Dickinson, L. C., & Lapidot, A. (1979) *J. Am. Chem. Soc. 101*, 1645−1654.

Nanthakumar, A., Fox, S., Murthy, N. N., Karlin, K. D., Ravi, N., Huynh, B. H., Orosz, R. D., Day, E. P., Hagen, K. S., & Blackburn, N. J. (1993) *J. Am. Chem. Soc. 115*, 8513−8514.

Powers, L., Chance, B., Ching, Y., & Angiolillo, P. (1981) *Biophys. J. 34*, 465−498.

Powers, L., Lauraeus, M., Reddy, K. S., Chance, B., & Wikström, M. (1994) *Biochim. Biophys. Acta 1183*, 504−512.

Puustinen, A., Finel, M., Haltia, T., Gennis, R. B., & Wikström, M. (1991) *Biochemistry 30*, 3936−3942.

Puustinen, A., Morgan, J. E., Verkhovsky, M., Thomas, J. W., Gennis, R. B., & Wikström, M. (1992) *Biochemistry 31*, 10363−10369.

Reedy, B. J., & Blackburn, N. J. (1994) *J. Am. Chem. Soc. 116*, 1924−1931.

Reinhammar, B., Malkin, R., Jensen, P., Karlsson, B., Andreasson, L.-E., Aasa, R., Vänngård, T., & Malmström, B. G. (1980) *J. Biol. Chem. 255*, 5000−5003.

Rich, P. R. (1995) *Austral. J. Plant Physiol. (*in press).

Roberts, J. E. (1982) Ph.D. Thesis, Northwestern University, Evanston, IL.

Rousseau, D. L., Ching, T.-c., & Wang, J. (1993) *J. Bioenerg. Biomembr. 25*, 165−176.

Santana, M., Kunst, F., Hullo, M. F., Rappoport, G., Danchin, A., & Glaser, P. (1992) *J. Biol. Chem. 267*, 10225−10231.

Sanyal, I., Karlin, K. D., Strange, R. W., & Blackburn, N. J. (1993) *J. Am. Chem. Soc. 115*, 11259−11270.

Saraste, M. (1990) *Q. Rev. Biophys. 23*, 331−366.

Scott, R. A., Li, P. M., & Chan, S. I. (1988) *Ann. N.Y. Acad. Sci. 550*, 53−58.

Scott, M. J., Lee, S. C., & Holm, R. H. (1994) *Inorg. Chem. 33*, 4651−4662.

Scott, M. J., Zhang, H. H., Lee, S. C., Hedman, B., Hodgson, K. O., & Holm, R. H. (1995) *J. Am. Chem. Soc. 117*, 568−569.

Shaw, R. W., Hansen, R. E., & Beinert, H. (1978) *Biochim. Biophys. Acta 504*, 187−199.

Strange, R. W., Blackburn, N. J., Knowles, P. F., & Hasnain, S. S. (1987) *J. Am. Chem. Soc. 109*, 7157−7162.

Surerus, K. K., Oertling, W. E., Fan, C., Gurbiel, R. J., Einarsdottir, O., Antholine, W. E., Dyer, R. B., Hoffman, B. M., Woodruff, W. H., & Fee, J. A. (1992) *Proc. Natl. Acad. Sci.* USA *89*, 3195−3199.

Thomas, J. W., Calhoun, M. W., Lemieux, L. J., Puustinen, A., Wikström, M., Alben, J. O., & Gennis, R. B. (1994) *Biochemistry 33*, 13013−13021.

van Camp, H. L., Sands, R. H., & Fee, J. A. (1981) *J. Chem. Phys. 75*, 2098−2107.

van Gelder, B. F., & Beinert, H. (1969) *Biochim. Biophys. Acta 189*, 1−24.

Verkhovsky, M. I., Morgan, J. E., & Wikström, M. (1992) *Biochemistry 31*, 11860−11863.

Werst, M. M., Davoust, C. E., & Hoffmann, B. M. (1991) *J. Am. Chem. Soc. 113*, 1533−1538.

Wikström, M. (1988) *Ann. N.Y. Acad. Sci. 550*, 199−206.

Wikström, M. (1989) *Nature 338*, 776−778.

Wikström, M., Krab, K., & Saraste, M. (1981) *Cytochrome Oxidase—A Synthesis*, Academic Press, New York.

Wikström, M., Bogachev, A., Finel, M., Morgan, J. E., Puustinen, A., Raitio, M., Verkhovskaya, M. L., & Verkhovsky, M. I. (1994) *Biochim. Biophys. Acta 1187*, 106−111.

Wilson, D. F., Erecinska, M., & Owen, C. S. (1976) *Arch. Biochem. Biophys. 175*, 160−173.

Woodruff, W. H. (1993) *J. Bioenerg. Biomembr. 25*, 177−188.

BI950918G